

Acoustic Waves in Baffled Combustion Chamber with Radial and Circumferential Blades

Danning You,* David D. Ku,† and Vigor Yang‡
 Georgia Institute of Technology, Atlanta, Georgia 30327-0150

DOI: 10.2514/1.B34923

A linear acoustic analysis has been conducted to study the combustion instability characteristics of three-dimensional baffled combustion chambers. The theoretical formulation is based on a generalized wave equation. Normal mode expansion and spatial averaging techniques are implemented to solve for the acoustic motions in the chamber. Several specific effects of radial and circumferential baffles, and the mechanisms by which baffles eliminate combustion instabilities, are presented. Longitudinalization of transverse waves inside baffle compartments, restriction of velocity fluctuations near the injector face, and reduction in oscillation frequency are studied systematically. The effects of mean flow, temperature nonuniformities, and combustion response on the baffle design and stability behaviors are investigated. Potential destabilizing influences of baffles are found to be the concentration of acoustic pressure at the injector face and of acoustic velocity near the baffle tips, as well as their ensuing interactions with local combustion processes.

Nomenclature

\bar{a}	= speed of sound in two-phase mixture
A_d	= acoustic admittance function [Eq. (4)]
C	= normal mode function coefficient [Eq. (21) or (30)]
C_f	= coefficient, Eq. (12)
C_h	= coefficient, Eq. (12)
C_Y	= coefficient, Eq. (32)
E	= defined in Eq. (48) or (55)
\mathcal{F}	= momentum equation source term
f	= boundary condition in wave equation [Eq. (3)] or frequency
G_h	= defined in Eq. (82)
G_{pq}	= defined in Eq. (52)
h	= source term in wave equation [Eq. (2)]
H_{mn}	= defined in Eq. (51)
I	= defined in Eqs. (60)–(63)
J_m	= m th order Bessel function of the first kind
k_{mn}	= eigenvalue of (m, n) th mode
L	= chamber length
L_b	= baffle blade length
\bar{L}_b	= normalized baffle blade length, L_b/R_c
M	= total number of modes in main chamber
\mathbf{n}	= unit outward normal vector
\mathcal{P}	= energy equation source term
p	= pressure
Q	= total number of modes in baffle compartments
r	= radial coordinate
\mathbf{r}	= position vector
R_b	= radius of center baffle compartment
R_c	= radius of main chamber
t	= time
\mathbf{u}	= velocity of the gas phase
u	= axial velocity
v	= radial velocity

w	= circumferential velocity
x	= axial coordinate
y	= transverse coordinate
Y_m	= m th-order Bessel function of the second kind
Z	= impedance
α	= axial wave number [Eq. (18) or (27)]
α_b	= ratio of sound speeds, \bar{a}_b/\bar{a}_c
β	= reflection coefficient
γ	= specific heat ratio for mixture
δ_{kl}	= Kronecker delta
η	= series coefficient of Fourier-type expansion
θ	= circumferential coordinate
ρ	= density of two-phase mixture
ψ_{mn}	= normal mode function of (m, n) th mode
Ω	= frequency

Overscripts, Superscripts, and Subscripts

b	= baffle compartment
c	= main chamber
I	= injector face
m	= circumferential direction mode in main chamber
N	= chamber nozzle
n	= radial direction mode in main chamber
p	= circumferential direction mode in baffle compartments
q	= radial direction mode in baffle compartments
T	= transverse plane
μ	= μ th baffle compartment
$-$	= mean quantity
\prime	= perturbation quantity
$\hat{}$	= fluctuation amplitude
$+$	= downstream running wave
$-$	= upstream running wave

I. Introduction

COMBUSTION instabilities have been encountered in many propulsion system development programs, including liquid rocket engines [1–3], gas turbine engines [4], and solid rocket motors [5,6]. They are characterized by an energy feedback loop between acoustic oscillations and combustion responses, but can be addressed through chamber design. For liquid-propellant rocket engines, injector face baffles are widely used to provide a stabilizing effect on transverse flow oscillations [7]. Figure 1 shows a typical baffle configuration consisting of flat plates extending into the combustion chamber perpendicularly from the injector face, arranged in a radial and/or circumferential pattern. Radial baffles are oriented radially

Presented as Paper 2005-930 at the 43rd AIAA Aerospace Sciences Meeting and Exhibit, Reno, Nevada, 10–13 January 2005; received 18 January 2013; revision received 16 April 2013; accepted for publication 21 April 2013; published online 2 July 2013. Copyright © 2013 by Vigor Yang. Published by the American Institute of Aeronautics and Astronautics, Inc., with permission. Copies of this paper may be made for personal or internal use, on condition that the copier pay the \$10.00 per-copy fee to the Copyright Clearance Center, Inc., 222 Rosewood Drive, Danvers, MA 01923; include the code 1533-3876/13 and \$10.00 in correspondence with the CCC.

*Research Engineer, Siemens Power. Member AIAA.

†Graduate Research Assistant. Student Member AIAA.

‡William R. T. Oakes Professor and Chair, School of Aerospace Engineering; vigor@gatech.edu. Fellow AIAA.

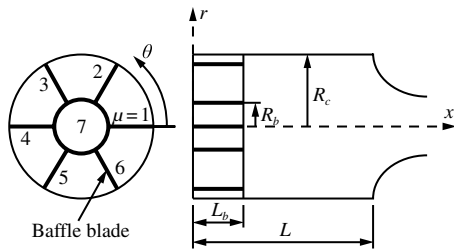


Fig. 1 Schematic of a seven-baffle combustion chamber.

outward from the center of the injector face; circumferential baffles are circular baffles of constant radius.

Several experimental investigations have produced results that lend valuable insight into the stabilizing effect of baffles. Early studies on the damping effect of baffles were limited to cold or non-reacting flow experiments [8–10]. Wieber [8] studied the stabilization effects of various baffle patterns in a combustion chamber with no mean flow. The radial baffles distorted the acoustic mode shapes by obstructing flow motion in the tangential direction and, hence, damped the transverse oscillations much more effectively than the longitudinal oscillations. The orientation of baffles with respect to the chamber acoustic field was found to be important. Later reacting flow experiments have yielded results applicable to practical rocket engines. Laudien et al. [11] conducted both cold-flow and hot-flow tests to study the effect of various passive instability-control devices such as Helmholtz resonators and injector-face baffles. Radial baffles with an odd number of blades were more effective than those with an even number of blades in suppressing transverse instabilities. For example, a three-bladed baffle was shown to damp the first and second tangential modes, whereas a four-bladed baffle had no effect on the second tangential mode. Furthermore, the decay rate of the transverse oscillations grew with increasing baffle length. More recent studies have been focused on active control of instabilities [12,13]. The results of the present work could be used to facilitate the development of these means of control.

Oefelein and Yang [14] gave a comprehensive review of the experimental studies of baffle design performed under the F-1 engine development program. More recently, Lee et al. [15] investigated the effect of gaps on acoustic damping with injector-formed baffles. Optimal gaps between injectors were found to maximize acoustic damping due to random acoustic reflections and increased viscous dissipation. The baffle length requirements (and related thermal cooling problems) could be reduced by optimizing injector gaps. Lubarsky et al. [16] studied the suppression of tangential instability by insertion of an asymmetric baffle through a slit in the wall of a combustion chamber. Partial insertion (10–30% of the chamber diameter) of the baffle produced complete damping of the first tangential mode. It was concluded that the instability suppressing mechanism was an acoustic phenomenon. The effect of shifting the flame zone from the injector face appeared to be limited.

Three main mechanisms have been proposed to explain the stabilizing effect of baffles [17–19]: 1) modification of the acoustic properties of the combustion chamber through reduction of the frequencies and amplitudes of transverse oscillations; 2) protection of sensitive combustion processes from acoustic flow motion in the chamber; and 3) dissipation of acoustic wave energy through vortex shedding and visco-acoustic interactions near the baffle blades. A detailed review of the existing experimental and theoretical studies up to the mid-1990s can be found in [19]. Wicker et al. [19] developed a general theoretical framework for treating both linear and nonlinear acoustic waves in baffled combustion chambers. Their results clearly demonstrated the importance of the first two stabilizing mechanisms. Inside baffle compartments, the transverse acoustic waves in the combustion chamber were longitudinalized, a phenomenon which becomes more pronounced with increased baffle length. The acoustic velocity was severely limited inside the baffle compartments. Large variations in the acoustic velocity, however, were observed immediately downstream of the baffle. The ensuing modifications of the acoustic field in the flame zone thus affected the system stability

characteristics by changing the local combustion response. The reduced oscillation frequencies also exerted a direct influence on the stability contingent upon the frequency dependence of the combustion response. Conditions for the existence of limit cycles were obtained, along with explicit formulas for the oscillation amplitudes and frequencies, in terms of linear and nonlinear parameters.

Analytical approaches to date have only treated configurations with radial blades in the chamber. In addition, the effects of mean flow and combustion–acoustic coupling have largely been neglected. In practice, many rocket engines have both radial and circumferential baffles for stabilization. The latter help restrict radial modes of instability [3,20,21] and are often arranged in the region where the radial velocity amplitude is maximal. Several numerical studies have been performed recently to treat both radial and circumferential blades. Quinlan et al. [22] developed a numerical code that predicts the stability of a combustion chamber with baffles and acoustic cavities. The velocity potential was first obtained through an eigenfunction expansion and then used as a basis to determine the pressure interaction index and complex combustion response through an iterative technique. Feng et al. [23] examined instabilities in the YF-960 rocket engine using a finite-volume method. Two different baffle configurations were considered: 1) three radial blades with a circular hub, and 2) six radial blades with a circular hub. Quinlan et al. [24] numerically verified the experimental findings of Lubarsky et al. [16] on the effects of asymmetric baffles. The calculated acoustic frequencies matched experimental data closely, and the 10% partial insertion was shown to be capable of disrupting the first spinning tangential mode. It was also found that increasing the baffle thickness decreased the oscillation frequencies.

The present study extends an earlier approach described in [19] to theoretically investigate the acoustic waves in chambers containing both radial and circumferential baffles, as shown schematically in Fig. 1. The nonuniformity of the mean flowfield is accommodated in a generalized framework. A large variation in temperature often occurs as the mixture moves from the baffle compartments to the main combustion chamber downstream. The ensuing change in the speed of sound in the chamber has a significant impact on the acoustic wave characteristics. This phenomenon is incorporated in the formulation, and its effect on the chamber stability characteristics is studied. The response of unsteady combustion to local acoustic oscillations is modeled using both velocity- and pressure-coupled response functions [25]. Following the methodology developed in [19], a combined modal expansion and spatial averaging technique is applied to solve the system of equations. Sample calculations are performed to examine the effects of geometry, mean-flow variations, and combustion response on the stability of baffled combustion chambers. In addition, mechanisms by which baffles eliminate combustion instabilities are explored.

II. Theoretical Formulation

A. Wave Equation

The acoustic motions in a chamber can be described by a generalized wave equation [19,25,26]. The conservation equations of mass, momentum, and energy are first formulated for the mixture in the combustion chamber. Each dependent variable is then decomposed as the sum of the mean and fluctuating components. After substituting them in the conservation equations and rearranging the result, a wave equation to first order is derived:

$$\nabla^2 p' - \frac{1}{a^2} \frac{\partial^2 p'}{\partial t^2} = h \quad (1)$$

The source term h has the form

$$h = h_I + h_{II} + h_{III} \quad (2)$$

where

$$\begin{aligned}
 h_I = & -\nabla \left(\bar{\rho} \frac{\partial \mathbf{u}'}{\partial t} \right) - \nabla [\bar{\rho} (\bar{\mathbf{u}} \cdot \nabla) \mathbf{u}'] - \nabla [\bar{\rho} (\mathbf{u}' \cdot \nabla) \bar{\mathbf{u}}] \\
 & - \nabla \left[\frac{p'}{\bar{a}^2} (\bar{\mathbf{u}} \cdot \nabla) \bar{\mathbf{u}} \right] + \frac{1}{\bar{a}^2} \frac{\partial}{\partial t} (\bar{\mathbf{u}} \cdot \nabla p') + \frac{1}{\bar{a}^2} \frac{\partial}{\partial t} (\mathbf{u}' \cdot \nabla \bar{p}) \\
 & + \frac{\bar{\gamma}}{\bar{a}^2} \frac{\partial}{\partial t} (\bar{p} \nabla \cdot \mathbf{u}') + \frac{1}{\bar{a}^2} \frac{\partial}{\partial t} (p' \nabla \cdot \bar{\mathbf{u}}) \quad (2a)
 \end{aligned}$$

$$h_{II} = \nabla \left[\frac{\bar{\rho} s'}{C_p} (\bar{\mathbf{u}} \cdot \nabla) \bar{\mathbf{u}} \right] \quad (2b)$$

$$h_{III} = -\frac{1}{\bar{a}^2} \frac{\partial}{\partial t} p' + \nabla \mathcal{F}' \dot{Q}' \quad (2c)$$

The first term h_I represents the linear gas dynamic effects. The second term h_{II} arises from entropy fluctuations. The third term h_{III} includes two-phase interactions, viscous dissipation, and combustion heat release.

The boundary condition for the wave equation is set using the gradient of p' , obtained by taking the scalar product of the outward normal vector with the perturbed momentum equations:

$$\begin{aligned}
 \mathbf{n} \cdot \nabla p' = & -f = \mathbf{n} \\
 & \cdot \left[-\bar{\rho} \frac{\partial \mathbf{u}'}{\partial t} - \bar{\rho} (\bar{\mathbf{u}} \cdot \nabla) \mathbf{u}' - \bar{\rho} (\mathbf{u}' \cdot \nabla) \bar{\mathbf{u}} - \rho' (\bar{\mathbf{u}} \cdot \nabla) \bar{\mathbf{u}} + \mathcal{F}' \right] \quad (3)
 \end{aligned}$$

Typically, this condition is treated using an acoustic admittance function A_d , which relates the local velocity fluctuation to its pressure counterpart:

$$A_d = \mathbf{n} \cdot \frac{\mathbf{u}' / \bar{a}}{p' / \bar{\gamma} \bar{p}} \quad (4)$$

If the volumetric and boundary source terms are absent (i.e., $h = f = 0$), the undamped wave equation for pressure in classical acoustics is recovered.

B. Mode Expansion and Spatial Averaging in the Transverse Plane

Because of the geometric complexity associated with baffles, a direct treatment of the wave equation subject to the boundary conditions appears to be a formidable challenge. The oscillatory field is best constructed for the baffle compartments and the main chamber separately, and then matched at the interface to determine the acoustic waves over the entire chamber. For situations commonly observed in most practical rocket engines in which the mean-flow Mach number and variation of mean pressure in the radial and circumferential directions are both small, the frequencies and spatial structures of unsteady motions on a transverse plane deviate only slightly from the classical acoustic field obtained for the same geometry as the combustion chamber but without any source terms. Thus, the solution to the wave equation can be faithfully approximated by a synthesis of the normal transverse acoustic modes [26]. Provisions are made to allow large variations in mean-flow properties in the axial direction. For linear analysis, all acoustic variables are assumed to vary in a time-harmonic fashion. The acoustic pressure can be expressed as a series of eigenfunctions for oscillations on the transverse plane, with the axial variations expressed as the expansion coefficients [19]

$$p'(\mathbf{r}, t) = e^{i\Omega t} \sum_{m=0}^{\infty} \sum_{n=0}^{\infty} [\hat{\eta}_{mn}(x) \psi_{mn}(\theta, r)] \quad (5)$$

where Ω stands for the complex frequency of the oscillations. The eigenfunction ψ_{mn} , also called the normal mode, satisfies the Helmholtz equation on the transverse plane,

$$\nabla_T^2 \psi_{mn} + k_{mn}^2 \psi_{mn} = 0 \quad (6)$$

where k_{mn} is the wave number of the normal mode ψ_{mn} . The double indices m and n correspond to the spatial variations in the circumferential and radial directions, respectively. Equation (6) is subject to the following boundary condition for a rigid surface along the combustor wall:

$$\mathbf{n} \cdot \nabla_T \psi_{mn} = 0 \quad (7)$$

The transverse Laplacian operation ∇_T^2 in cylindrical coordinates is defined as

$$\nabla_T^2 = \frac{1}{r} \frac{\partial}{\partial r} \left(r \frac{\partial}{\partial r} \right) + \frac{1}{r^2} \frac{\partial^2}{\partial \theta^2} \quad (8)$$

Multiplying Eq. (6) by p' and Eq. (1) by ψ_{mn} , subtracting the latter from the former, and then integrating over the cross section results in

$$\begin{aligned}
 \iint \left[p' \nabla_T^2 \psi_{mn} + p' k_{mn}^2 \psi_{mn} - \psi_{mn} \nabla^2 p' + \psi_{mn} \frac{1}{\bar{a}^2} \frac{\partial^2 p'}{\partial t^2} \right] ds \\
 = - \iint \psi_{mn} h \, ds \quad (9)
 \end{aligned}$$

Application of Green's theorem and substitution of boundary conditions from Eqs. (3) and (7) into Eq. (9) yields

$$\begin{aligned}
 \iint \left[p' k_{mn}^2 \psi_{mn} - \psi_{mn} \frac{\partial^2 p'}{\partial x^2} + \psi_{mn} \frac{1}{\bar{a}^2} \frac{\partial^2 p'}{\partial t^2} \right] ds \\
 = - \iint \psi_{mn} h \, ds - \oint \psi_{mn} f_T \, dl \quad (10)
 \end{aligned}$$

where the line integral $\oint dl$ is performed along the surface boundary of the cross section, and $f_T = -\mathbf{n} \cdot \nabla_T p'$. Substituting Eq. (5) into Eq. (10) and rearranging the result leads to

$$\begin{aligned}
 \frac{d^2 \hat{\eta}_{mn}}{dx^2} + \left(\frac{\Omega^2}{\bar{a}^2} - k_{mn}^2 \right) \hat{\eta}_{mn} \\
 = \frac{1}{\iint (\psi_{mn})^2 ds} \left[\iint \psi_{mn} \hat{h} \, ds + \oint \psi_{mn} \hat{f}_T \, dl \right] \quad (11)
 \end{aligned}$$

The source terms \hat{h} and \hat{f}_T are functions of both the mean and oscillatory flow properties. The latter consists of a series of transverse acoustic modes. Because of the disparity in the length scales associated with these modes, the acoustic mode coupling in the source terms in Eq. (11) can be reasonably ignored. It can be shown that the cross-coupling terms are much smaller, and only the specific mode of concern dominates. Thus, to facilitate the formulation, the surface and line integrals on the right-hand side of Eq. (11) can be modeled as the products of the axial variation $\hat{\eta}_{mn}$ and coefficients $C_{h,mn}$ and $C_{f,mn}$, respectively, which include all the distributed and surface effects at a given cross section through spatial averaging:

$$\iint \psi_{mn} \hat{h} \, ds = C_{h,mn} \hat{\eta}_{mn}(x) \quad \oint \psi_{mn} \hat{f}_T \, dl = C_{f,mn} \hat{\eta}_{mn}(x) \quad (12)$$

Equation (11) now reduces to a second-order ordinary differential equation with constant coefficients whose solution $\hat{\eta}_{mn}(x)$ takes the form

$$\hat{\eta}_{mn}(x) = p_{mn}^+ \exp(i\alpha_{mn}^+ x) + p_{mn}^- \exp(i\alpha_{mn}^- x) \quad (13)$$

where p_{mn}^+ and p_{mn}^- are the complex amplitudes of the upstream and downstream traveling waves, respectively. The axial wave number α_{mn}^\pm is related to the frequency Ω , eigenvalue k_{mn} , and the source-term coefficients by

$$(\alpha_{mn}^\pm)^2 = \frac{\Omega^2}{\bar{a}^2} - k_{mn}^2 - C_{h,mn}(\alpha_{mn}^\pm, \dots) - C_{f,mn}(\alpha_{mn}^\pm, \dots) \quad (14)$$

Through normal transverse-mode expansion, the solution to the wave equation has been given in the form of Eq. (5), with the eigenfunction provided by Eq. (6). The axial variation expressed in Eq. (13) is derived by applying spatial averaging over each transverse plane. The acoustic pressure in each cell can thus be explicitly expressed by combining these results:

$$p'(\mathbf{r}, t) = e^{i\Omega t} \sum_{m=0}^{\infty} \sum_{n=0}^{\infty} [\psi_{mn}(\theta, r) (p_{mn}^+ e^{i\alpha_{mn}^+ x} + p_{mn}^- e^{i\alpha_{mn}^- x})] \quad (15)$$

The axial velocity fluctuation u' can be obtained from the linearized axial momentum equation:

$$u'(\mathbf{r}, t) = -\frac{1}{\bar{\rho}} \sum_{m=0}^{\infty} \sum_{n=0}^{\infty} \times \left[e^{i\Omega t} \psi_{mn}(\theta, r) \left(\frac{\alpha_{mn}^+ p_{mn}^+ e^{i\alpha_{mn}^+ x}}{\Omega + \bar{u}_c \alpha_{mn}^+} + \frac{\alpha_{mn}^- p_{mn}^- e^{i\alpha_{mn}^- x}}{\Omega + \bar{u}_c \alpha_{mn}^-} \right) \right] \quad (16)$$

C. Acoustic Waves in Baffle Compartments and Main Chamber

The flow conditions in an operational liquid rocket engine are complicated. To reduce the complexity arising in analyzing the acoustic field, the current work deals only with cases in which the mean-flow properties such as temperature and Mach number are different in the baffle compartments and main chamber, but uniform within each section. The oscillatory fields in these two regions are treated separately and then matched at the interface to solve for the acoustic motions in the entire combustor, as shown schematically in Figs. 1 and 2.

1. Main Chamber

If the acoustic admittance at the wall is assumed to be zero, the spatially varying function $\hat{\eta}_{mn}$ in the main chamber can be written as

$$\hat{\eta}_{mn}(x) = p_{mn}^+ \exp[i\alpha_{mn}^+(x-L)] + p_{mn}^- \exp[i\alpha_{mn}^-(x-L)] \quad (17)$$

where

$$\alpha_{mn}^{\pm} = \frac{1}{1 - \bar{M}_c^2} \left[\mp \frac{\bar{M}_c \Omega}{\bar{a}_c} + \sqrt{\frac{\Omega^2}{\bar{a}_c^2} - (1 - \bar{M}_c^2) k_{mn}^2} \right] \quad (18)$$

The subscript c stands for properties in the main chamber. The acoustic boundary condition at the nozzle entrance can be characterized by an admittance function defined as

$$A_{d,N} = \frac{u'/\bar{a}}{p'/\gamma\bar{p}} \Big|_{x=L} \quad (19)$$

This leads to a relationship between the constant coefficients p_{mn}^+ and p_{mn}^- :

$$\beta_{mn} = \frac{p_{mn}^-}{p_{mn}^+} = -\frac{A_{d,N} + \bar{a}_c \alpha_{mn}^+ / (\Omega + \bar{u}_c \alpha_{mn}^+)}{A_{d,N} + \bar{a}_c \alpha_{mn}^- / (\Omega + \bar{u}_c \alpha_{mn}^-)} \quad (20)$$

The transverse eigenfunctions for the main chamber are expressed in terms of sinusoids and Bessel functions of the first kind,

$$\psi_{mn}(\theta, r) = \psi_{mn}^c(\theta, r) + C_{mn} \psi_{mn}^s(\theta, r) \quad (21)$$

where

$$\begin{aligned} \psi_{mn}^c(\theta, r) &= \cos(m\theta) J_m(k_{mn} r) \quad \text{and} \\ \psi_{mn}^s(\theta, r) &= \sin(m\theta) J_m(k_{mn} r) \end{aligned} \quad (22)$$

For a rigid chamber wall, the eigenvalue k_{mn} can be obtained from the following equation:

$$\frac{d}{dr} J_m(k_{mn} r) = 0 \quad \text{at} \quad r = R_c \quad (23)$$

The pressure wave in the main chamber can then be written as

$$p'_c(\mathbf{r}, t) = e^{i\Omega t} \sum_{m=0}^{\infty} \sum_{n=0}^{\infty} \left[\psi_{mn}(\theta, r) p_{mn}^+ \frac{e^{i\alpha_{mn}^+(x-L)} + \beta_{mn} e^{i\alpha_{mn}^-(x-L)}}{e^{i\alpha_{mn}^+(L_b-L)} + \beta_{mn} e^{i\alpha_{mn}^-(L_b-L)}} \right] \quad (24)$$

From the linearized x -momentum equation, the axial velocity fluctuation is obtained as follows:

$$u'_c(\mathbf{r}, t) = -\frac{e^{i\Omega t}}{\bar{\rho}_c} \sum_{m=0}^{\infty} \sum_{n=0}^{\infty} \times \left[\frac{\psi_{mn}(\theta, r) p_{mn}^+}{e^{i\alpha_{mn}^+(L_b-L)} + \beta_{mn} e^{i\alpha_{mn}^-(L_b-L)}} \left(\frac{\alpha_{mn}^+ e^{i\alpha_{mn}^+(x-L)} + \beta_{mn} \alpha_{mn}^- e^{i\alpha_{mn}^-(x-L)}}{\Omega + \bar{u}_c \alpha_{mn}^+} + \frac{\beta_{mn} \alpha_{mn}^- e^{i\alpha_{mn}^-(x-L)}}{\Omega + \bar{u}_c \alpha_{mn}^-} \right) \right] \quad (25)$$

2. Baffle Compartment

The solution to Eq. (11) for the baffle compartments takes the form

$$\hat{\eta}_{pq}^{\mu}(x) = p_{pq}^{+\mu} \exp(i\alpha_{pq}^{+\mu} x) + p_{pq}^{-\mu} \exp(i\alpha_{pq}^{-\mu} x) \quad (26)$$

where

$$\alpha_{pq}^{\pm\mu} = \frac{1}{1 - \bar{M}_b^2} \left[\mp \frac{\bar{M}_b \Omega}{\bar{a}_b} + \sqrt{\frac{\Omega^2}{\bar{a}_b^2} - (1 - \bar{M}_b^2) k_{pq}^2} \right] \quad (27)$$

The superscript μ , subscript b , and indices p and q stand for the μ th baffle compartment, properties in the baffle compartment, and spatial variations in the circumferential and radial directions, respectively. The acoustic boundary condition at the injector face is characterized by an admittance function defined as

$$A_{d,I} = \frac{u'/\bar{a}}{p'/\gamma\bar{p}} \Big|_{x=0} \quad (28)$$

This gives a relationship between the constant coefficients $p_{pq}^{+\mu}$ and $p_{pq}^{-\mu}$:

$$p_{pq}^{\mu} = \frac{p_{pq}^{-\mu}}{p_{pq}^{+\mu}} = -\frac{A_{d,I} + \bar{a}_b \alpha_{pq}^{+\mu} / (\Omega + \bar{u}_b \alpha_{pq}^{+\mu})}{A_{d,I} + \bar{a}_b \alpha_{pq}^{-\mu} / (\Omega + \bar{u}_b \alpha_{pq}^{-\mu})} \quad (29)$$

Owing to the boundary conditions associated with both radial and circumferential baffle blades, the eigenfunctions in the baffle compartments are distinct from their counterparts in [19], which deal only with radial blades. For the μ th baffle compartment, writing

$$\psi_{pq}^{\mu}(\theta, r) = \psi_{pq}^{\mu c}(\theta, r) + C_{pq}^{\mu} \psi_{pq}^{\mu s}(\theta, r) \quad (30)$$

the eigenfunction for the peripheral baffle compartments (e.g., $\mu = 1, 2, \dots, 6$ in Fig. 1) thus becomes

$$\begin{aligned} \psi_{pq}^{\mu c}(\theta, r) &= \cos\left(\frac{pN}{2}\theta\right) [J_{pN/2}(k_{pNq/2} r) + C_{Ypq} Y_{pN/2}(k_{pNq/2} r)] \\ \psi_{pq}^{\mu s}(\theta, r) &= 0 \end{aligned} \quad (31)$$

where N denotes the total number of radial baffle blades and Y is the Bessel function of the second kind. The coefficient C_{Ypq} is defined as

$$C_{Ypq} = -\left[\frac{dJ_{pN/2}(k_{pNq/2} r)/dr}{dY_{pN/2}(k_{pNq/2} r)/dr} \right]_{r=R_c} \quad (32)$$

The eigenvalues can be determined by applying the boundary condition, Eq. (7):

$$\left[\frac{dJ_{pN/2}(k_{pNq/2}r)}{dr} \Big|_{r=R_c} \cdot \frac{dY_{pN/2}(k_{pNq/2}r)}{dr} \Big|_{r=R_b} - \left[\frac{dJ_{pN/2}(k_{pNq/2}r)}{dr} \Big|_{r=R_b} \cdot \frac{dY_{pN/2}(k_{pNq/2}r)}{dr} \Big|_{r=R_c} \right] \right] = 0 \quad (33)$$

For the center baffle compartment ($\mu = 7$),

$$\begin{aligned} \psi_{pq}^{\mu c}(\theta, r) &= \cos(p\theta)J_p(k_{pq}r) \quad \text{and} \\ \psi_{pq}^{\mu s}(\theta, r) &= C_{pq}^{\mu} \sin(p\theta)J_p(k_{pq}r) \end{aligned} \quad (34)$$

The eigenvalue can be obtained by

$$\frac{d}{dr} J_p(k_{pq}r) = 0 \quad \text{at} \quad r = R_b \quad (35)$$

Therefore, the acoustic pressure and velocity waves in the baffle compartment can be expressed as

$$\begin{aligned} p'_\mu(\mathbf{r}, t) &= e^{i\Omega t} \sum_{p=0}^{\infty} \sum_{q=0}^{\infty} \left[\psi_{pq}^{\mu}(\theta, r) p_{pq}^{+\mu} \frac{e^{i\alpha_{pq}^{+\mu}x} + \beta_{pq}^{\mu} e^{i\alpha_{pq}^{-\mu}x}}{e^{i\alpha_{pq}^{+\mu}L_b} + \beta_{pq}^{\mu} e^{i\alpha_{pq}^{-\mu}L_b}} \right] \quad (36) \\ u'_\mu(\mathbf{r}, t) &= -\frac{e^{i\Omega t}}{\bar{\rho}_b} \sum_{p=0}^{\infty} \sum_{q=0}^{\infty} \\ &\times \left[\frac{\psi_{pq}^{\mu}(\theta, r) p_{pq}^{+\mu}}{e^{i\alpha_{pq}^{+\mu}L_b} + \beta_{pq,\mu}^{\mu} e^{i\alpha_{pq}^{-\mu}L_b}} \left(\frac{\alpha_{pq}^{+\mu} e^{i\alpha_{pq}^{+\mu}x}}{\Omega + \bar{u}_b \alpha_{pq}^{+\mu}} + \frac{\beta_{pq,\mu}^{\mu} \alpha_{pq}^{-\mu} e^{i\alpha_{pq}^{-\mu}x}}{\Omega + \bar{u}_b \alpha_{pq}^{-\mu}} \right) \right] \quad (37) \end{aligned}$$

3. Matching at the Interface

The oscillatory fields in the baffle compartments and main chamber are matched at the interface ($x = L_b$) to determine the wave

$$\begin{cases} E_{pq}^{\mu c} = \int_{R_b}^{R_c} \int_{2\pi(\mu-1)/N}^{2\pi\mu/N} (\psi_{pq}^{\mu c})^2 r \, dr \, d\theta & \text{(peripheral compartments)} \\ E_{pq}^{\mu s} = \int_0^{R_b} \int_0^{2\pi} (\psi_{pq}^{\mu s})^2 r \, dr \, d\theta \quad \text{and} \quad E_{pq}^{\mu s} = \int_0^{R_b} \int_0^{2\pi} (\psi_{pq}^{\mu s})^2 r \, dr \, d\theta & \text{(center compartments)} \end{cases} \quad (48)$$

characteristics in the entire system. The matching conditions require continuities of mass and momentum fluxes throughout the interface:

Mass flux is given by

$$(\rho_\mu u_\mu)|_{x=L_b^-} = (\rho_c u_c)|_{x=L_b^+} \quad (38)$$

Momentum flux is given by

$$(p_\mu + \rho_\mu u_\mu^2)|_{x=L_b^-} = (p_c + \rho_c u_c^2)|_{x=L_b^+} \quad (39)$$

Decomposing the variables into mean and fluctuating components and subsequently linearizing results in

$$(\bar{\rho}_\mu u'_\mu + \rho'_\mu \bar{u}_\mu)|_{x=L_b^-} = (\bar{\rho}_c u'_c + \rho'_c \bar{u}_c)|_{x=L_b^+} \quad (40)$$

$$(p'_\mu + 2\bar{\rho}_\mu \bar{u}_\mu u'_\mu + \rho'_\mu \bar{u}_\mu^2)|_{x=L_b^-} = (p'_c + 2\bar{\rho}_c \bar{u}_c u'_c + \rho'_c \bar{u}_c^2)|_{x=L_b^+} \quad (41)$$

The velocity and density disturbances can be related to the pressure fluctuations through the acoustic impedance and the speed of sound as follows:

$$u' \sim p' / \bar{\rho} \bar{a}, \quad \rho' \sim p' / \bar{a}^2 \quad (42)$$

The order of magnitude of each term in Eqs. (40) and (41) becomes, respectively,

$$\bar{\rho} \bar{u} u' \sim p' / \bar{a}, \quad \rho' \bar{u} \sim \bar{M} p' / \bar{a} \quad (43)$$

$$\bar{\rho} \bar{u} u' \sim p' \cdot \bar{M}, \quad \rho' \bar{u}^2 \sim p' \cdot \bar{M}^2 \quad (44)$$

For low-speed flows, such as those encountered in most liquid rocket engines, terms with order of magnitude \bar{M}^2 can be neglected. Equation (41) can be simplified to

$$(p'_\mu + 2\bar{\rho}_\mu \bar{u}_\mu u'_\mu)|_{x=L_b^-} = (p'_c + 2\bar{\rho}_c \bar{u}_c u'_c)|_{x=L_b^+} \quad (45)$$

Multiplying Eq. (45) by $\psi_{pq}^{\mu c} r dr d\theta$ and $\psi_{pq}^{\mu s} r dr d\theta$, respectively, and integrating the results over each corresponding baffle compartment, the following is obtained using the orthogonality of eigenfunctions:

$$\sum_{m'=0}^{\infty} \sum_{n'=0}^{\infty} \left[p_{m'n'}^{+\mu} \left(\iint \psi_{m'n'} \psi_{pq}^{\mu c} r \, dr \, d\theta \right) R_{m'n'} \right] = p_{pq}^{+\mu} \cdot E_{pq}^{\mu c} \cdot S_{pq}^{\mu} \quad (46)$$

$$\begin{aligned} \sum_{m'=0}^{\infty} \sum_{n'=0}^{\infty} \left[p_{m'n'}^{+\mu} \left(\iint \psi_{m'n'} \psi_{pq}^{\mu s} r \, dr \, d\theta \right) R_{m'n'} \right] \\ = p_{pq}^{+\mu} \cdot E_{pq}^{\mu s} \cdot C_{pq}^{\mu} \cdot S_{pq}^{\mu} \end{aligned} \quad (47)$$

where

$$R_{m'n'} = (1 - 2\bar{u}_c H_{m'n'}) \quad (49)$$

$$S_{pq}^{\mu} = (1 - 2\bar{u}_b G_{pq}^{\mu}) \quad (50)$$

and

$$\begin{aligned} H_{mn} &= \frac{1}{e^{i\alpha_{mn}^+(L_b-L)} + \beta_{mn} e^{i\alpha_{mn}^-(L_b-L)}} \\ &\cdot \left[\frac{\alpha_{mn}^+ e^{i\alpha_{mn}^+(L_b-L)}}{\Omega + \bar{u}_c \alpha_{mn}^+} + \frac{\beta_{mn} \alpha_{mn}^- e^{i\alpha_{mn}^-(L_b-L)}}{\Omega + \bar{u}_c \alpha_{mn}^-} \right] \end{aligned} \quad (51)$$

$$G_{pq}^{\mu} = \frac{1}{e^{i\alpha_{pq}^{+\mu}L_b} + \beta_{pq}^{\mu} e^{i\alpha_{pq}^{-\mu}L_b}} \cdot \left[\frac{\alpha_{pq}^{+\mu} e^{i\alpha_{pq}^{+\mu}L_b}}{\Omega + \bar{u}_b \alpha_{pq}^{+\mu}} + \frac{\beta_{pq}^{\mu} \alpha_{pq}^{-\mu} e^{i\alpha_{pq}^{-\mu}L_b}}{\Omega + \bar{u}_b \alpha_{pq}^{-\mu}} \right] \quad (52)$$

Similarly, multiplying Eq. (40) by $\psi_{mn}^c r dr d\theta$ and $\psi_{mn}^s r dr d\theta$, respectively, and integrating the results over the entire cross section of the main chamber yields

$$p_{mn}^+ \cdot E_{mn}^c \cdot U_{mn} = \sum_{p=0}^{\infty} \sum_{q=0}^{\infty} \sum_{\mu=1}^N \left[V_{pq}^{\mu} P_{pq}^{+\mu} \left(\iint \psi_{pq}^{\mu c} \psi_{mn}^c r dr d\theta \right) \right] \quad (53)$$

$$p_{mn}^+ C_{mn} \cdot E_{mn}^s \cdot U_{mn} = \sum_{p=0}^{\infty} \sum_{q=0}^{\infty} \sum_{\mu=1}^N \left[V_{pq}^{\mu} P_{pq}^{+\mu} \left(\iint \psi_{pq}^{\mu c} \psi_{mn}^s r dr d\theta \right) \right] \quad (54)$$

where

$$E_{mn}^c = \int_0^{R_c} \int_0^{2\pi} (\psi_{mn}^c)^2 r dr d\theta \quad \text{and} \quad (55)$$

$$E_{mn}^s = \int_0^{R_c} \int_0^{2\pi} (\psi_{mn}^s)^2 r dr d\theta$$

$$U_{mn} = (H_{mn} - \bar{M}_c / \bar{a}_c) \quad (56)$$

$$V_{pq}^{\mu} = (G_{pq}^{\mu} - \bar{M}_b / \bar{a}_b) \quad (57)$$

Equation (21) is substituted into Eqs. (46) and (47) to obtain

$$p_{pq}^{+\mu} = \frac{1}{E_{pq}^{\mu c} \cdot S_{pq}^{\mu}} \sum_{m'=0}^{\infty} \sum_{n'=0}^{\infty} [P_{m'n'}^+ (I_{pq,m'n'}^{\mu c,c} + C_{m'n'} I_{pq,m'n'}^{\mu c,s}) R_{m'n'}] \quad (58)$$

$$p_{pq}^{\mu s} = \frac{1}{E_{pq}^{\mu s} \cdot S_{pq}^{\mu}} \sum_{m'=0}^{\infty} \sum_{n'=0}^{\infty} [P_{m'n'}^+ (I_{pq,m'n'}^{\mu s,c} + C_{m'n'} I_{pq,m'n'}^{\mu s,s}) R_{m'n'}] \quad (59)$$

where the coefficients are defined as

$$I_{pq,m'n'}^{\mu c,c} = \iint \psi_{m'n'}^{\mu c} \psi_{pq}^{\mu c} r dr d\theta \quad (60)$$

$$I_{pq,m'n'}^{\mu c,s} = \iint \psi_{m'n'}^{\mu c} \psi_{pq}^{\mu s} r dr d\theta \quad (61)$$

$$I_{pq,m'n'}^{\mu s,c} = \iint \psi_{m'n'}^{\mu s} \psi_{pq}^{\mu c} r dr d\theta \quad (62)$$

$$I_{pq,m'n'}^{\mu s,s} = \iint \psi_{m'n'}^{\mu s} \psi_{pq}^{\mu s} r dr d\theta \quad (63)$$

and

$$p_{pq}^{\mu s} = C_{pq}^{\mu} p_{pq}^{+\mu} \quad (64)$$

Plugging Eq. (30) into Eqs. (53) and (54) results in

$$p_{mn}^+ = \frac{1}{E_{mn}^c U_{mn}} \sum_{p=0}^{\infty} \sum_{q=0}^{\infty} \sum_{\mu=1}^N [V_{pq}^{\mu} P_{pq}^{+\mu} (I_{pq,mn}^{\mu c,c} + C_{pq}^{\mu} I_{pq,mn}^{\mu c,s})] \quad (65)$$

$$p_{mn}^s = \frac{1}{E_{mn}^s U_{mn}} \sum_{p=0}^{\infty} \sum_{q=0}^{\infty} \sum_{\mu=1}^N [V_{pq}^{\mu} P_{pq}^{+\mu} (I_{pq,mn}^{\mu s,c} + C_{pq}^{\mu} I_{pq,mn}^{\mu s,s})] \quad (66)$$

where

$$p_{mn}^s = C_{mn} p_{mn}^+ \quad (67)$$

Equations (58) and (59) are substituted into Eqs. (66) and (67) to obtain

$$p_{mn}^+ = \sum_{p=0}^{\infty} \sum_{q=0}^{\infty} \sum_{\mu=1}^N \sum_{m'=0}^{\infty} \sum_{n'=0}^{\infty} \frac{V_{pq}^{\mu} R_{m'n'}}{E_{mn}^c U_{mn} S_{pq}^{\mu}} \times \left[p_{m'n'}^+ \left(\frac{I_{pq,mn}^{\mu c,c} I_{pq,m'n'}^{\mu c,c}}{E_{pq}^{\mu c}} + \frac{I_{pq,mn}^{\mu s,c} I_{pq,m'n'}^{\mu s,c}}{E_{pq}^{\mu s}} \right) + p_{m'n'}^s \left(\frac{I_{pq,mn}^{\mu c,s} I_{pq,m'n'}^{\mu c,s}}{E_{pq}^{\mu c}} + \frac{I_{pq,mn}^{\mu s,s} I_{pq,m'n'}^{\mu s,s}}{E_{pq}^{\mu s}} \right) \right] \quad (68)$$

$$p_{mn}^s = \sum_{p=0}^{\infty} \sum_{q=0}^{\infty} \sum_{\mu=1}^N \sum_{m'=0}^{\infty} \sum_{n'=0}^{\infty} \frac{V_{pq}^{\mu} R_{m'n'}}{E_{mn}^s U_{mn} S_{pq}^{\mu}} \times \left[p_{m'n'}^+ \left(\frac{I_{pq,mn}^{\mu c,s} I_{pq,m'n'}^{\mu c,c}}{E_{pq}^{\mu c}} + \frac{I_{pq,mn}^{\mu s,c} I_{pq,m'n'}^{\mu s,c}}{E_{pq}^{\mu s}} \right) + p_{m'n'}^s \left(\frac{I_{pq,mn}^{\mu c,s} I_{pq,m'n'}^{\mu s,s}}{E_{pq}^{\mu c}} + \frac{I_{pq,mn}^{\mu s,s} I_{pq,m'n'}^{\mu s,s}}{E_{pq}^{\mu s}} \right) \right] \quad (69)$$

The combination of the preceding two equations leads to a system of equations in terms of the series coefficients for the main chamber,

$$[F] \begin{bmatrix} p^+ \\ p^s \end{bmatrix} = \begin{bmatrix} f_{11}^a & f_{12}^a & \cdots & f_{1M}^a & f_{11}^b & f_{12}^b & \cdots & f_{1M}^b \\ f_{21}^a & f_{22}^a & \cdots & f_{2M}^a & f_{21}^b & f_{22}^b & \cdots & f_{2M}^b \\ \vdots & \vdots \\ f_{M1}^a & f_{M2}^a & \cdots & f_{MM}^a & f_{M1}^b & f_{M2}^b & \cdots & f_{MM}^b \\ f_{11}^c & f_{12}^c & \cdots & f_{1M}^c & f_{11}^d & f_{12}^d & \cdots & f_{1M}^d \\ f_{21}^c & f_{22}^c & \cdots & f_{2M}^c & f_{21}^d & f_{22}^d & \cdots & f_{2M}^d \\ \vdots & \vdots \\ f_{M1}^c & f_{M2}^c & \cdots & f_{MM}^c & f_{M1}^d & f_{M2}^d & \cdots & f_{MM}^d \end{bmatrix} \begin{bmatrix} p_1^+ \\ p_2^+ \\ \vdots \\ p_M^+ \\ p_1^s \\ p_2^s \\ \vdots \\ p_M^s \end{bmatrix} = 0 \quad (70)$$

where

$$f_{k,k'}^a = \sum_{\mu=1}^N \sum_{l=0}^Q \frac{V_l^{\mu} R_{k'}}{E_k^c U_k S_l^{\mu}} \left(\frac{I_{l,k}^{\mu c,c} I_{l,k'}^{\mu c,c}}{E_l^{\mu c}} + \frac{I_{l,k}^{\mu s,c} I_{l,k'}^{\mu s,c}}{E_l^{\mu s}} \right) - \delta_{kk'} \quad (71)$$

$$f_{k,k'}^b = \sum_{\mu=1}^N \sum_{l=0}^Q \frac{V_l^{\mu} R_{k'}}{E_k^s U_k S_l^{\mu}} \left(\frac{I_{l,k}^{\mu c,s} I_{l,k'}^{\mu c,s}}{E_l^{\mu c}} + \frac{I_{l,k}^{\mu s,s} I_{l,k'}^{\mu s,s}}{E_l^{\mu s}} \right) \quad (72)$$

$$f_{k,k'}^c = \sum_{\mu=1}^N \sum_{l=0}^Q \frac{V_l^{\mu} R_{k'}}{E_k^c U_k S_l^{\mu}} \left(\frac{I_{l,k}^{\mu c,s} I_{l,k'}^{\mu c,c}}{E_l^{\mu c}} + \frac{I_{l,k}^{\mu s,c} I_{l,k'}^{\mu s,c}}{E_l^{\mu s}} \right) \quad (73)$$

$$f_{k,k'}^d = \sum_{\mu=1}^N \sum_{l=0}^Q \frac{V_l^{\mu} R_{k'}}{E_k^s U_k S_l^{\mu}} \left(\frac{I_{l,k}^{\mu c,s} I_{l,k'}^{\mu s,s}}{E_l^{\mu c}} + \frac{I_{l,k}^{\mu s,s} I_{l,k'}^{\mu s,s}}{E_l^{\mu s}} \right) - \delta_{kk'} \quad (74)$$

To simplify the notation, the double indices such as pq have been replaced by single indices; that is, mn by k , pq by l , and $m'n'$ by k' . In this system, the limits of k and l are M and Q , respectively, representing the numbers of eigenfunctions of Eqs. (21) and (30) in the series expansions for the main chamber and baffle compartments, respectively. For nontrivial solutions to $[p^+ \ p^s]^T$, the determinant of the coefficient matrix of Eq. (70) must vanish, giving

$$\det |F(\Omega_{mn})| = 0 \quad (75)$$

Although no simple expression for Ω can be derived from Eq. (75), the functional dependence can be graphically investigated over some region in the complex Ω plane. By plotting the magnitude of $\det |F|$ over the frequency region of interest and graphically identifying the points at which $\det |F|$ vanishes, a close estimation of the modal frequencies can be achieved. Using these values as initial guesses, each eigenvalue may be found to a desired level of accuracy by secant iteration of the complex $\det |F|$ over the complex frequency plane. The series coefficients $[p^+ \ p^-]^T$ can be determined from Eq. (70) once the frequency is known.

III. Results and Discussion

A. Combustion Chambers with Radial Baffles

To focus on the effect of mean-flow properties on the acoustic field, a relatively simple geometry, a cylindrical chamber with only three radial baffles, as shown in Fig. 2, is considered. The influence of baffle length, mean-flow Mach number, and the temperature ratio between the baffle compartment and main chamber on the acoustic field in the entire chamber is studied. The situation with combustion response is also examined. The chamber geometry and operating parameters are summarized in Table 1.

The first case provides basic understanding of baffle effects on the acoustic field in the combustion chamber. No heat release is considered to avoid complications arising from combustion response. Figure 3 presents the acoustic pressure and velocity contours of the first tangential mode at various cross sections. Here, the n th transverse mode refers to the wave characteristics in the far downstream region of the baffled chamber that most closely resembles the n th transverse mode in an equivalent unbaffled chamber. To solve for this n th mode, the number M in Eq. (70) is set to be n . The mode numbers in baffle compartments in the circumferential and radial directions are selected to be $p = 0, 1, 2, \dots, 10$ and $q = 0, 1, 2, \dots, 10$. These numbers are also used in the subsequent cases. The wave pattern resembles a classical tangential mode in the downstream end of the chamber, but becomes distorted near the baffle tips. It finally reaches a symmetric

Table 1 Chamber dimensions and operating parameters

Case	L/R_c	L_b/R_c	\bar{a}_b/\bar{a}_c	\bar{M}_b	\bar{M}_c
1	2.5	0.4	1	0	0
2	2.5	0-0.8	1	0	0
3	2.5	0.4	0.5	0	0
4	2.5	0.4	1.5	0	0
5	2.5	0.4	0.5-1.5	0	0
6	2.5	0.4	1	0-0.5	0-0.5

pattern with respect to the $\theta = 0$ blade at the injector face. The magnitudes of acoustic velocities in the baffle compartments are substantially limited. It is well established [2,3] that the transverse velocity components exert a strong effect on such combustion processes as atomization, mixing and flame stabilization and spreading. The decrease in the acoustic velocity magnitudes helps stabilize a system with a velocity-sensitive combustion response.

Figure 4 shows the pressure and velocity distributions on various azimuthal planes ($\theta = 0, 60, 180$ and 240 deg). High-amplitude pressure oscillations are clearly observed near the injector face. A major factor contributing to this phenomenon is the longitudinalization of transverse acoustic waves, which creates a pressure antinode at the injector face [19]. This can be a potential source of instability if the combustion is pressure sensitive in that region. At $\theta = 240$ deg where there is a baffle blade, large pressure gradients appear near the baffle tips, thereby inducing intense acoustic velocities. The resultant velocity-coupled combustion response may destabilize the system.

1. Effect of Baffle Length

The effect of baffle length on the acoustic field is examined. As a specific example, case 2 is considered. Figure 5 shows the acoustic pressure fields of the first transverse mode for three different baffle lengths. When the baffle length is increased, the acoustic wave is progressively longitudinalized in the baffle compartments, especially between $\theta = 120$ and 240 deg, as shown in Fig. 5. Such a change can strongly affect system stability through the combustion response to pressure oscillations.

Dranovsky et al. [3] developed an approximate relationship between the acoustic frequencies and baffle length. The derivation is given in the Appendix. Using the notation employed in the present work, the frequency of the acoustic waves in the baffled chamber can be written as

$$\tan\left(\frac{R_c k_{mn} \bar{L}_b \bar{\Omega}_{mn}}{\alpha_b}\right) = \frac{S_c \bar{\rho}_c \bar{a}_c \bar{\Omega}_{mn}}{S_b \bar{\rho}_b \bar{a}_b \sqrt{1 - \bar{\Omega}_{mn}^2}} \quad (76)$$

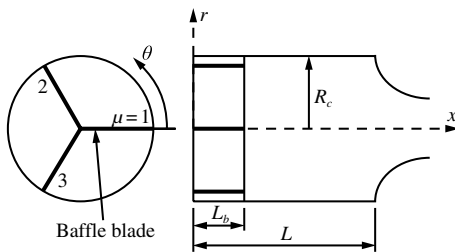


Fig. 2 Schematic of a three-baffle combustion chamber.

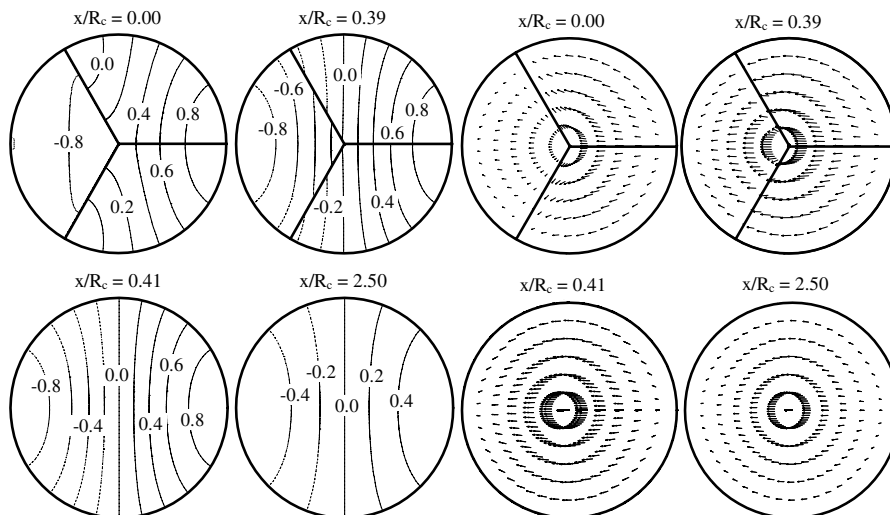


Fig. 3 Acoustic pressure and velocity distributions of first tangential mode at various cross sections in a three-baffle chamber (case 1: $L_b/R_c = 0.4$ and $\bar{a}_b/\bar{a}_c = 1.0$).

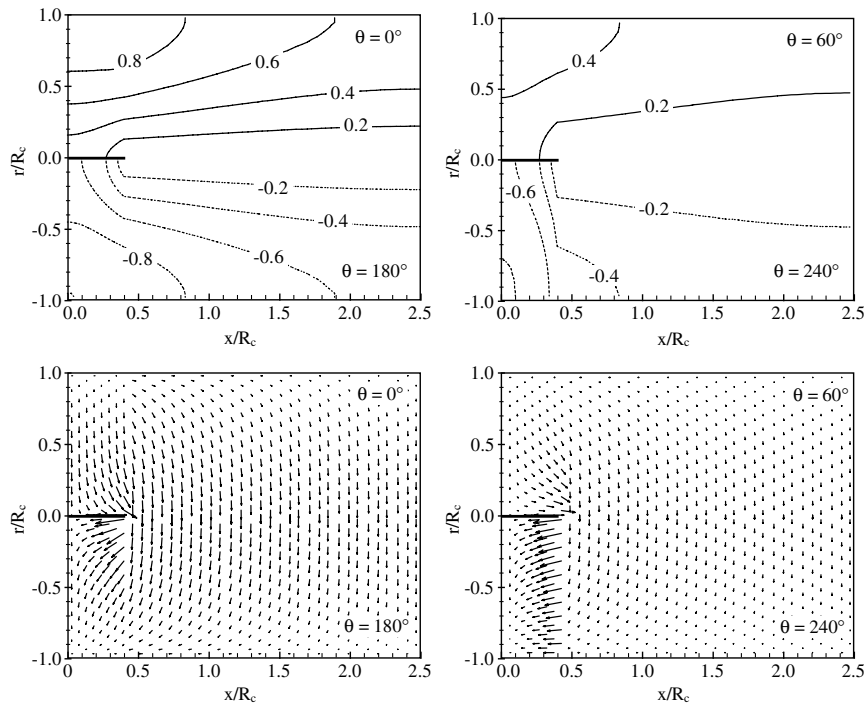


Fig. 4 Acoustic pressure and velocity distributions of first tangential mode on various azimuthal planes (constant θ) planes in a three-baffle chamber (case 1: $L_b/R_c = 0.4$ and $\bar{a}_b/\bar{a}_c = 1.0$).

where $\bar{L}_b = L_b/R_c$ denotes the normalized baffle length, $\bar{\Omega}_{mn} = \Omega/(k_{mn}\bar{a}_c)$ the normalized frequency of the (m, n) th transverse mode, and $\alpha_b = \bar{a}_b/\bar{a}_c$ the ratio of sound velocity in the baffle compartment to that in the main chamber. Equation (76) indicates that the acoustic frequency depends intimately on the baffle length, ratio of speeds of sound, acoustic impedance $\bar{\rho}\bar{a}$, and chamber geometry. As the baffle length tends to zero, the transverse-mode frequency approaches that of an unbaffled combustion chamber.

Figure 6 shows the frequency of the first tangential mode, normalized by that of an unbaffled chamber ($R_c k_{mn} = 1.84$) as a function of normalized baffle length. The gas properties in the baffle

compartments are assumed to be identical to those in the main chamber; that is, $\bar{a}_b = \bar{a}_c$ and $S_b\bar{\rho}_b\bar{a}_b = S_c\bar{\rho}_c\bar{a}_c$. The solid line is the analytical solution predicted by Eq. (76), and the symbols are the results from the present analysis. The normalized frequency decreases with increasing baffle length due to enhanced longitudinalization of the acoustic waves in the baffle compartments. The analytical solution assumes complete longitudinalization and thus overpredicts the reduction in frequency with increasing baffle length. A similar observation of frequency decrease was made previously [19] for transverse waves in both two-dimensional and three-dimensional chambers. This phenomenon can be attributed to the fact that the acoustic wavefront must travel over a greater distance in a baffled chamber because the wave front must turn 180 deg around the baffle. The turning of the wavefront can also be observed in the velocity vector plot, as shown in Figure 4.

The baffle-induced decrease of oscillation frequency may significantly affect combustion response through its modulated frequency. If the unbaffled acoustic frequency is lower than the frequency at which the combustion response retains its maximum $f_{c,max}$ (as illustrated by scenario 1 in Fig. 7), then adding baffles has a stabilizing effect. The situation, however, becomes different if the frequency exceeds $f_{c,max}$ (scenario 2). Baffles may exert either a stabilizing or a destabilizing effect, depending on their length.

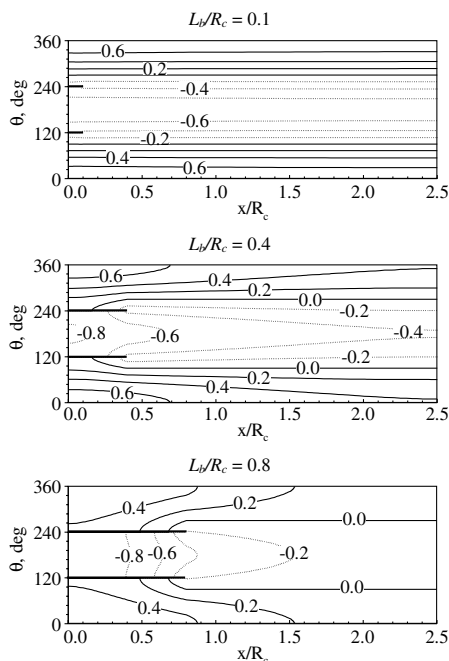


Fig. 5 Effect of baffle length on acoustic pressure field in a three-baffle chamber, first transverse mode (case 2: $\bar{a}_b/\bar{a}_c = 1.0$).

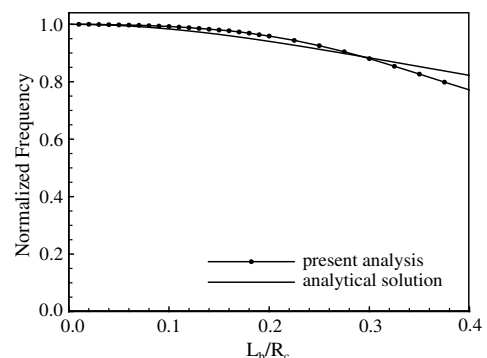


Fig. 6 Effect of baffle length on oscillation frequency in a three-baffle chamber, first transverse mode (case 2: $\bar{a}_b/\bar{a}_c = 1.0$).

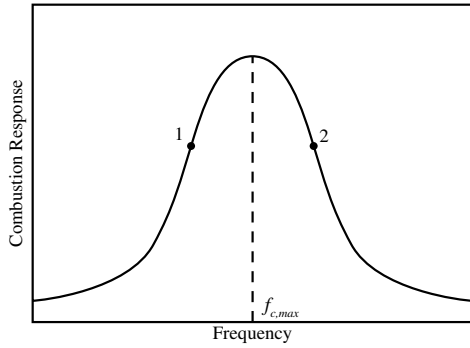


Fig. 7 A hypothetical frequency spectrum of combustion response.

2. Effect of Temperature Variation

Cases 3 and 4 in Table 1 are concerned with the effect of a nonuniform mean temperature distribution. Such a temperature effect is mainly exhibited by the variation of the sound speed in the chamber. The case of $\alpha_b < 1$ is typical for main combustion chambers, whereas $\alpha_b > 1$ commonly occurs in preburners in which cold propellants are injected downstream of the baffles [3]. Examples of such preburners include those on the RD-120 and RD-170 engines

employing oxygen-rich staged-combustion cycles. Figure 8 presents the acoustic pressure and velocity contours of the first tangential mode at various cross sections for $\alpha_b = 0.5$ corresponding to a temperature ratio of 0.25. The acoustic wave structure within baffle compartments is similar to the situation with a uniform temperature distribution (case 1), shown in Fig. 3. The velocity oscillation, however, decreases significantly toward the downstream end of the chamber. The overall velocity magnitude in the baffle compartments is also reduced. This phenomenon can be explained by evaluating the characteristic acoustic impedance $\bar{\rho} \bar{a}$. The higher impedance in the main chamber leads to lower velocity fluctuations.

In gas generators or preburners, the combustion products are often cooled by injection of cold propellants to prevent adverse heat transfer to turbine blades. The ratio of sound speeds becomes greater than unity. Case 4 ($\alpha_b = 1.5$) was selected for a sample calculation. Figure 9 shows the acoustic pressure and velocity fields. The pressure oscillations at various cross sections behave like a perfect first tangential mode in the downstream end of the chamber, but are attenuated closer to the injector face. In contrast to case 3, the acoustic impedance is lower downstream, resulting in higher velocity oscillations in the main chamber and lower velocity oscillations near the injector face.

Figure 10 compares the acoustic pressure distributions on the $r = R/2$ cylindrical surface for the two different ratios of sound

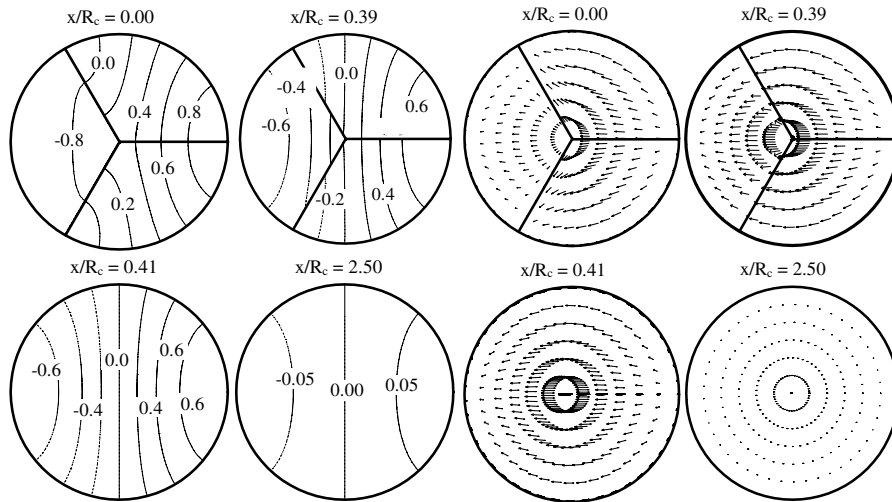


Fig. 8 Acoustic pressure and velocity distributions of first tangential mode at various cross sections in a three-baffle chamber (case 3: $L_b/R_c = 0.4$ and $\bar{a}_b/\bar{a}_c = 0.5$).

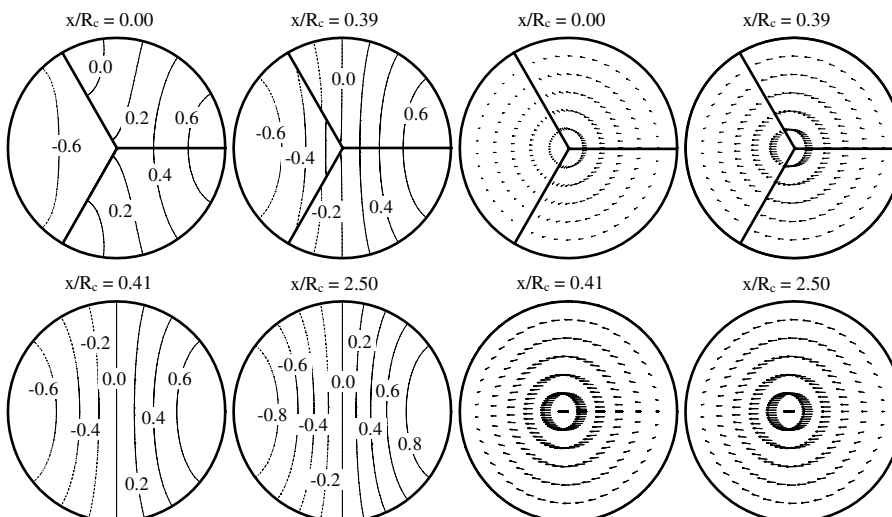


Fig. 9 Acoustic pressure and velocity distributions of first tangential mode at various cross sections in a three-baffle chamber (case 4: $L_b/R_c = 0.4$ and $\bar{a}_b/\bar{a}_c = 1.5$).

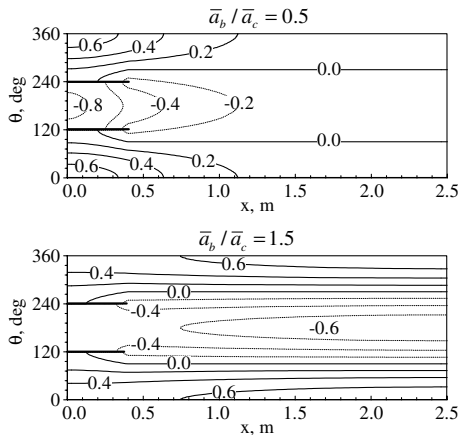


Fig. 10 Acoustic pressure distributions of first tangential mode on $r = R/2$ cylindrical surface in a three-baffle chamber of different baffle lengths ($L_b/R_c = 0.4$).

speeds. For $\alpha_b = 0.5$, the amplitude of pressure fluctuations decrease significantly as the wave propagates downstream, presenting a longitudinal behavior in baffle compartments. For $\alpha_b = 1.5$, on the other hand, the pressure oscillations behave like the first tangential mode in the entire chamber. Such a contrast can be explained as follows. The magnitudes of the reflection and transmission of a plane wave propagating across the interface between two different media (baffle compartments and main chamber) are given by

$$\frac{p_{\mu}^{-}}{p_{\mu}^{+}} = \frac{(\bar{\rho}_c \bar{a}_c)/(\bar{\rho}_b \bar{a}_b) - 1}{(\bar{\rho}_c \bar{a}_c)/(\bar{\rho}_b \bar{a}_b) + 1} \quad \text{and} \quad \frac{p_c'}{p_{\mu}^{+}} = \frac{2(\bar{\rho}_c \bar{a}_c)/(\bar{\rho}_b \bar{a}_b)}{(\bar{\rho}_c \bar{a}_c)/(\bar{\rho}_b \bar{a}_b) + 1} \quad (77)$$

Substituting the value of the sound-speed ratio into the preceding equations, the following is obtained:

$$\frac{p_c'}{p_{\mu}^{+}} = \begin{cases} 0.67, & \alpha_b = 0.5 \\ 2, & \alpha_b = 1.5 \end{cases} \quad (78)$$

Equation (78) shows that the amplitude of the transverse wave transmitted across the interface is reduced for case 3 ($\alpha_b = 0.5$) but amplified for case 4 ($\alpha_b = 1.5$). The result is consistent with that shown in Fig. 10. The pressure oscillations decrease near the injector face for case 4. The same trend was observed with velocity oscillations in Fig. 8 due to reduced wave reflection.

Figure 11 shows the effect of the sound-speed ratio on the normalized oscillation frequency in a three-baffle chamber for the first transverse mode. The frequency increases with increasing sound-speed ratio. The trend can be also predicted qualitatively by Eq. (76). For a given speed of sound in the main chamber, the acoustic

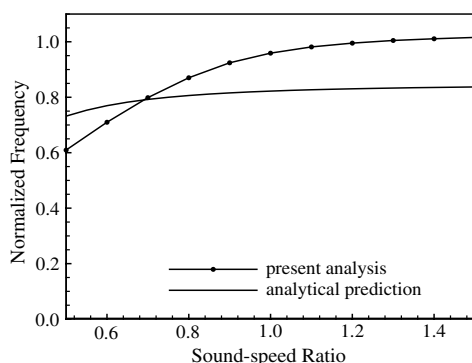


Fig. 11 Effect of sound-speed ratio on oscillation frequency in a three-baffle chamber, first transverse mode (case 5: $L_b/R_c = 0.4$).

frequency increases with increasing α_b . The existence of baffles has a stronger effect on both the oscillation frequency and mode shape of the acoustic field in the main combustion chamber (where $\alpha_b < 1$) than in a gas generator (where $\alpha_b > 1$ due to downstream injection cooling).

3. Effect of Mean Flow Velocity

The mean-flow Mach number in a rocket combustion chamber is typically so low that it has negligible impact on the linear acoustic field. The mean flow, however, may play an important role in determining nonlinear stability behaviors and energy transfer [27–29]. Acoustic oscillations can receive energy from the mean flow and grow into finite amplitude limit cycles [30]. Figure 12 shows the effect of the mean-flow Mach number on the oscillation frequency in a three-baffle chamber for the first transverse mode. The frequency decreases as the Mach number increases. The modifications in the acoustic pressure and velocity distributions by the mean flow appear to be negligible in the present case.

4. Effect of Combustion Response

All the preceding cases are pure acoustic problems; the effect of combustion response has not yet been considered. The interactions between unsteady heat release and flow oscillations are discussed here, which can be generally modeled by the source term h_{III} in Eq. (2c). Ignoring the gas dynamic effect and focusing only on unsteady heat release,

$$h = -(\gamma - 1)i\Omega \dot{Q}'/\bar{a}^2 \quad (79)$$

the oscillatory heat-release rate \dot{Q}' is related to local pressure and velocity fluctuations as follows [25],

$$\frac{\dot{Q}'}{\bar{Q}} = R_p \frac{p'}{\bar{p}} + R_u \frac{u'}{\bar{a}} + R_v \frac{v'}{\bar{a}} + R_w \frac{w'}{\bar{a}} \quad (80)$$

where R_p and R_u , R_v , and R_w are complex variables commonly referred to as the pressure- and velocity-coupled response functions, respectively. Substitution of the oscillatory flow properties from Eqs. (15) and (16) into Eq. (80) and application of Eq. (12) yields

$$C_{h,mn}^{\pm} = \iint \psi_{mn} G_{h,mn}^{\pm} ds \quad (81)$$

where

$$G_{h,mn}^{\pm} = -\frac{i(\gamma - 1)\Omega \bar{Q}}{\bar{\rho} \bar{a}^2} \cdot \left[\frac{R_p \bar{\rho}}{\bar{p}} \psi_{mn} - \frac{R_u \alpha_{mn}^{\pm} \psi_{mn}}{\bar{a}(\Omega + \bar{u} \alpha_{mn}^{\pm})} + \frac{iR_v}{\bar{a}(\Omega + \bar{u} \alpha_{mn}^{\pm})} \frac{\partial \psi_{mn}}{\partial r} - \frac{mR_w \psi_{mn}}{\bar{a}r(\Omega + \bar{u} \alpha_{mn}^{\pm})} \right] \quad (82)$$

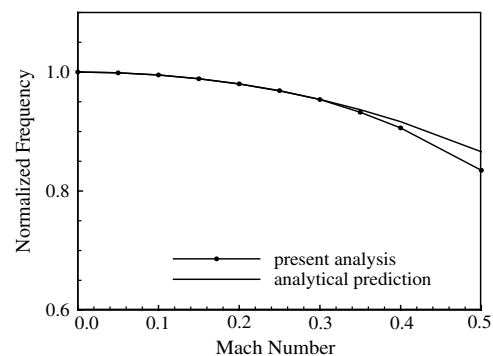


Fig. 12 Effect of mean-flow Mach number on oscillation frequency in a three-baffle chamber, first transverse mode (case 6: $L_b/R_c = 0.4$ and $\bar{a}_b/\bar{a}_c = 1.0$).

Table 2 Chamber geometry and combustion response functions for different cases

Case	Unbaffled chamber		Chamber with three radial baffles				
	7	8	9	10	11	12	13
L_b/R_c	0	0.1	0.4	0.8	0.1	0.4	0.8
R_p	0.5-0.5i	0.5-0.5i	0.5-0.5i	0.5-0.5i	0	0	0
R_u	0	0	0	0	0.5-0.5i	0.5-0.5i	0.5-0.5i

The formulation is thus closed once the combustion response functions are known. Several empirical and analytical models, including time lag [25,30] and flame-response [31] models, have been developed and employed to represent the combustion responses. In the present study, constant response functions are applied within the baffle compartments.

The sample calculations are performed for a chamber with three radial baffles, as shown in Fig. 2. The sound-speed ratio α_b between the baffled compartments and main chamber is 0.75. Combustion heat release is assumed to be uniformly distributed within the baffle compartments. The inlet Mach number is 0.15. For comparison, the acoustic characteristics of an unbaffled chamber are calculated. The combustion zone spans a length of $L_{comb} = 0.4L$. The effect of baffle length is then investigated with different response functions. Table 2 summarizes the chamber geometries and operating conditions examined. The response functions R_p and R_u are chosen to ensure unstable responses with semi-arbitrary amplitudes.

Figure 13 shows the first tangential mode in the chamber without baffle blades (case 7). A pressure-coupled combustion response was applied in this case. Similar to case 3, the amplitude of the transverse wave across the interface was attenuated. The calculated imaginary part of the complex frequency was found to be negative, indicating that the oscillations were unstable.

Cases 8–10 involve three radial baffles. The acoustic pressure wave is longitudinalized in the baffle compartments to satisfy the boundary condition. Figure 14 depicts the acoustic pressure fields on the $r = R/2$ cylindrical surface for different baffle lengths. The calculated oscillations are unstable for all these cases due to the intensive pressure field near the injector face. Because pressure-sensitive combustion is responsible for the instability, such concentration of the pressure oscillation near the injector face further enhances the destabilizing effect.

Cases 11–13 treat velocity-coupled combustion responses. With $L_b/R_c = 0.1$ (case 11), the oscillations are unstable only for short

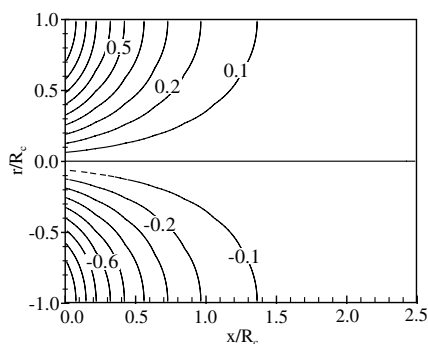


Fig. 13 Acoustic pressure distributions of first tangential mode on constant azimuthal planes ($\theta = 0$ and 180 deg) in an unbaffled chamber (case 7: $\bar{a}_b/\bar{a}_c = 0.75$ and $R_p = 0.5-0.5i$).

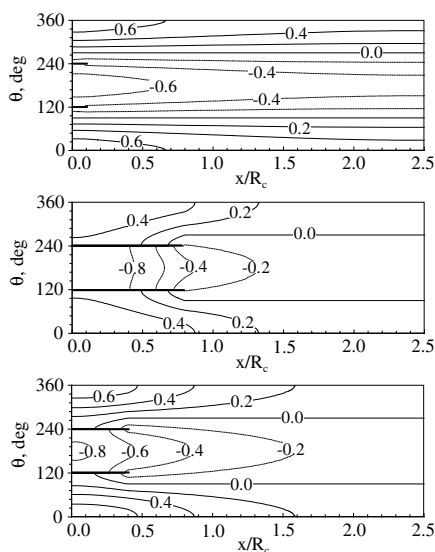


Fig. 14 Acoustic pressure distributions of first tangential mode on $r = R/2$ cylindrical surface in a three-baffle chamber (cases 8–10: $L_b/R_c = 0.1, 0.4$ and 0.8 , $\bar{a}_b/\bar{a}_c = 0.75$, and $R_p = 0.5-0.5i$).

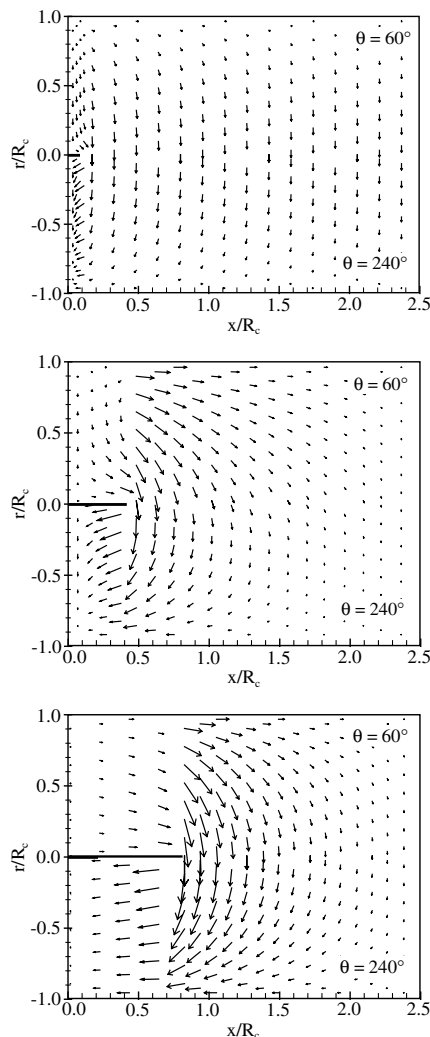


Fig. 15 Acoustic velocity distributions of first tangential mode on constant azimuthal planes in a three-baffle chamber (cases 11–13: $L_b/R_c = 0.1, 0.4$ and 0.8 , $\bar{a}_b/\bar{a}_c = 0.75$, and $R_u = 0.5-0.5i$).

Table 3 Chamber geometry and speed of sound of RD-120 main combustor

R_c , m	R_b , m	L , m	L_b , m	a , m/s
0.32	0.18	0.1872	0.03	1900

baffles. Longer baffles tend to stabilize oscillating motions. Figure 15 shows the acoustic velocity distributions on constant azimuthal planes. Large velocity fluctuations exist immediately downstream of the baffle blades in spite of their limited amplitudes inside the baffle compartments. Near the injector face, the combined effect of baffle length and higher acoustic impedance ($\alpha_b = 0.75$) tends to attenuate velocity fluctuations. Downstream of the baffle tips, however, the wave tuning along with decreased acoustic impedance gives rise to intensified velocity fluctuations. It is further observed that the velocity oscillations near the baffle tips are amplified with increasing baffle length. This may be attributed to the penetration of the blades into the chamber where the acoustic velocity inherently has a higher magnitude. In cases 12 and 13, the first tangential mode is unstable due to increased velocity fluctuations and subsequent combustion responses near the baffle tips.

B. Acoustic Field in a Chamber with Radial and Circumferential Baffles

The acoustic fields in chambers with both radial and circumferential baffles are studied. As an example, the main combustor of the RD-120 rocket engine is considered. It contains one center and six peripheral baffle compartments, as shown in Fig. 1. The chamber geometry and speed of sound are given in Table 3.

Figures 16–19 present the acoustic pressure and velocity fields of the first tangential, second tangential, first radial, and mixed first tangential–radial mode, respectively. The combustion chamber has a relatively short aspect ratio and baffle length compared to the three-baffle combustor studied earlier. The influence of the baffles on the acoustic field is thus not significant except for regions near the baffle blades. For both the transverse and radial modes, the transverse velocity oscillations decrease in the baffle compartments and then increase just downstream of the interface. If velocity-sensitive combustion response prevails in the near field around the baffle tips, then the baffles act as a destabilizing device. For the first and second tangential modes, the pressure and velocity fields in the center compartment near the injector face seem unaffected by the presence of the baffles. In the outer compartments, the pressure distribution has been modulated and the velocity distribution has improved. The opposite is observed for the first radial mode in Fig. 18. The pressure and velocity fields are intensified in the center compartment and

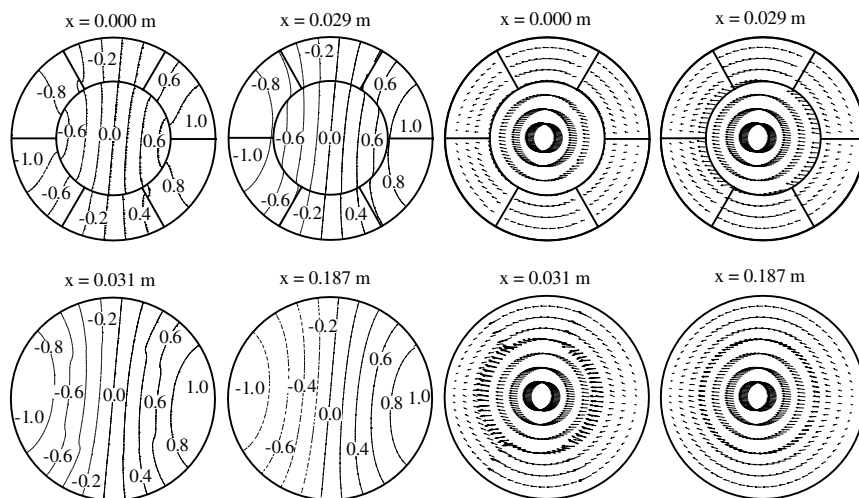


Fig. 16 Acoustic pressure and velocity distributions of first tangential mode at various cross sections in seven-baffle chamber (RD-120 main combustor).

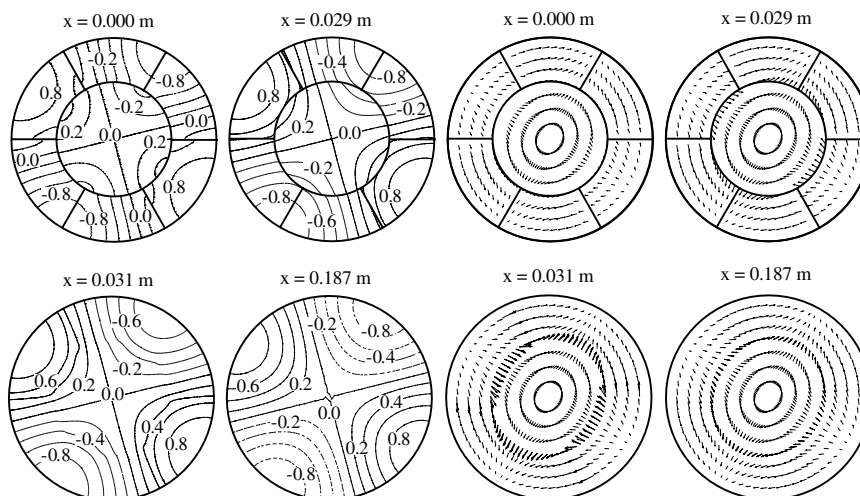


Fig. 17 Acoustic pressure and velocity distributions of second tangential mode at various cross sections in seven-baffle chamber (RD-120 main combustor).

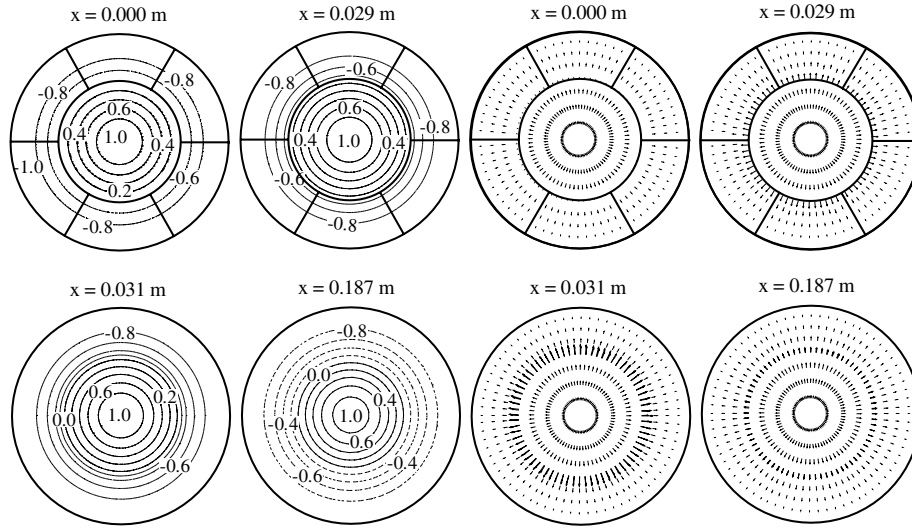


Fig. 18 Acoustic pressure and velocity distributions of first radial mode at various cross sections in seven-baffle chamber (RD-120 main combustor).

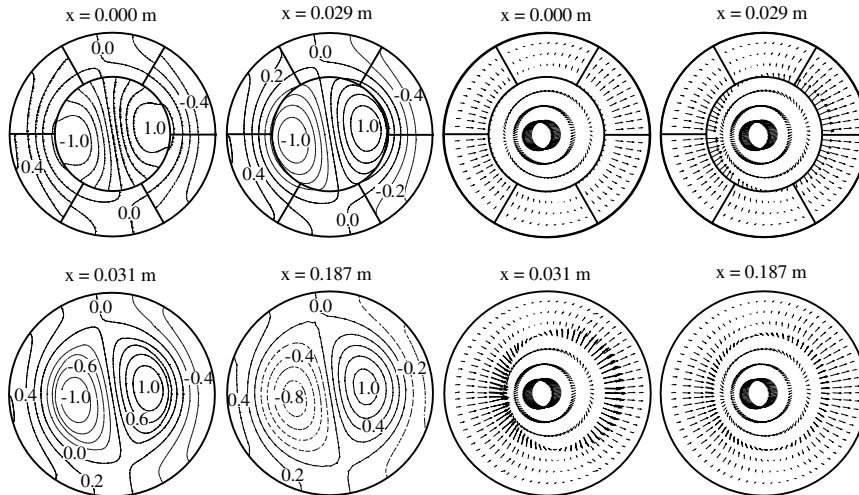


Fig. 19 Acoustic pressure and velocity distributions of mixed first tangential/first radial mode at various cross sections in seven-baffle chamber (RD-120 main combustor).

weakened in the peripheral compartments. Thus, the baffle arrangement could destabilize combustion for the first radial mode if the combustion response is velocity sensitive.

IV. Conclusions

A linear analysis of acoustic waves in baffled combustion chambers was performed using a perturbation–expansion technique. The formulation was based on a generalized wave equation derived from the conservation equations for a two-phase mixture, and includes effects of gas dynamics and combustion responses. Various underlying mechanisms by which baffles eliminate combustion instabilities in two-dimensional chambers are first explained, including longitudinalization of transverse waves within baffle compartments, restriction of velocity fluctuations near the injector face, and reduction in the oscillation frequency. Baffles are also found to present at least one potentially destabilizing effect: concentration of acoustic pressure near the injector face. For three-dimensional chambers with only radial baffles, similar effects of baffle blades on chamber stability are observed. Longitudinalization of acoustic waves, however, is not obvious in three-dimensional chambers with both radial and circumferential blades. For pure tangential modes, the acoustic pressure in the center baffle compartment remains almost identical to that in an unbaffled chamber. The pressure oscillations in the peripheral compartments are confined whereas the acoustic velocity is enhanced. The chamber stability characteristics depend on the sensitivities of the combustion response to acoustic motion. For a

pure radial mode, both pressure and velocity fluctuations increase in the center cavity, suggesting a destabilizing influence on the chamber stability.

Acknowledgments

This work was sponsored by the Air Force Office of Scientific Research under Contract No. FA-9550-10-1-0179. The support and encouragement provided by Dr. Mitat A. Birkan is gratefully acknowledged.

Appendix A: Frequencies of Acoustic Waves in Baffled Chambers

Recall Eqs. (15) and (16) for acoustic pressure and velocity. If the inhomogeneous term in the wave equation contains uniform mean flow only, the wave number α_{mn}^{\pm} can be determined by

$$\alpha_{mn}^{\pm} = \frac{1}{1 - \bar{M}^2} \left[\mp \frac{\bar{M}\Omega}{\bar{a}} + \sqrt{\frac{\Omega^2}{\bar{a}^2} - (1 - \bar{M}^2)k_{mn}^2} \right] \quad (A1)$$

A1. Pure Longitudinal Wave

For a pure longitudinal wave, $m = n = 0$, and $k_{mn} = 0$, Eq. (A1) simplifies to

$$(\alpha_{00}^{\pm})^2 = (k + M\alpha_{00}^{\pm})^2 \quad (\text{A2})$$

where $k = \Omega/\bar{a}$. With $\bar{M} = 0$,

$$\alpha_{00}^{\pm} = \mp k \quad (\text{A3})$$

An acoustic impedance function can be written as

$$Z = \frac{p'}{u'} = \bar{\rho} \bar{a} (R + iY) \quad (\text{A4})$$

where R and Y are the real and imaginary parts of the impedance, respectively. Note that the preceding definition does not include γ , as that in Eq. (28), in order to be consistent with [3] (p. 71). At the chamber inlet ($x = 0$), the impedance Z_0 is

$$Z_0 = \frac{p'}{u'} \Big|_{x=0} = -\bar{\rho} \bar{a} \frac{p^+ + p^-}{p^+ - p^-} \quad (\text{A5})$$

Equation (A5) can be rearranged to

$$p^- = \frac{\bar{Z}_0 + 1}{\bar{Z}_0 - 1} p^+ \quad (\text{A6})$$

where $\bar{Z}_0 = Z_0/\bar{\rho} \bar{a}$. At the combustor exit ($x = L$), the impedance Z_L becomes

$$Z_L = \frac{p'}{u'} \Big|_{x=L} = -\bar{\rho} \bar{a} \frac{p^+ + p^- e^{i2kL}}{p^+ - p^- e^{i2kL}} \quad (\text{A7})$$

Substitution of Eq. (A6) into Eq. (A7) results in

$$Z_L = \bar{\rho} \bar{a} \frac{\bar{Z}_0 + i \tan(kL)}{i\bar{Z}_0 \tan(kL) + 1} \quad (\text{A8})$$

Here Z_L is the transposed impedance of a chamber of length L with the inlet impedance Z_0 .

A2. Pure Transverse Wave

For a pure transverse wave without the mean-flow velocity, Eq. (A1) gives

$$\Omega = \bar{a} k_{mn} \quad (\text{A9})$$

where the eigenvalue k_{mn} is determined by either Eq. (23) or Eq. (33). With the inclusion of the mean flow at a Mach number M , the condition for a wave propagating at the lowest frequency becomes

$$\Omega/\bar{a} - k_{mn} \sqrt{1 - \bar{M}^2} = 0 \quad (\text{A10})$$

Rewriting Eq. (A10), the resonant frequency is defined as

$$f_{mn} = \frac{k_{mn} \bar{a}}{2\pi} \sqrt{1 - \bar{M}^2} \quad (\text{A11})$$

A3. Mixed Longitudinal-Transverse Wave

For a length L chamber with acoustically closed ends ($Z_0 \rightarrow \infty$, $Z_L \rightarrow \infty$) and in the absence of mean flow, the wave number becomes

$$\alpha_{mn} = l\pi/L \quad (\text{A12})$$

where l stands for the mode number in the axial direction. The wave number k can be determined by

$$k^2 = k_{mn}^2 + \alpha_{mn}^2 = k_{mn}^2 + (l\pi/L)^2 \quad (\text{A13})$$

Rearranging Eq. (A13), the natural frequencies of mixed longitudinal-transverse oscillations are

$$f_{lmn} = \frac{k_{mn} \bar{a}}{2\pi} \sqrt{1 + \left(\frac{l\pi}{Lk_{mn}}\right)^2} \quad (\text{A14})$$

To account for a nonzero mean-flow velocity, Eq. (A1) gives

$$(\alpha_{mn}^+ + \alpha_{mn}^-)(1 - \bar{M}^2) = 2\sqrt{\frac{\Omega^2}{\bar{a}^2} - (1 - \bar{M}^2)k_{mn}^2} \quad (\text{A15})$$

Substitution of Eq. (A12) into Eq. (A15) leads to the natural frequencies of mixed longitudinal-transverse modes with the effects of mean flow captured.

$$f_{lmn} = \frac{k_{mn} \bar{a}}{2\pi} (1 - \bar{M}^2) \sqrt{\frac{1}{1 - \bar{M}^2} + \left(\frac{l\pi}{Lk_{mn}}\right)^2} \quad (\text{A16})$$

A4. Waves in Chambers with Baffle Blades

The following assumptions are made:

- 1) The frequency is lower than the frequency of a purely transverse mode $_{mn}$.
- 2) Pure longitudinal oscillations are realized within baffle compartments.
- 3) Acoustic impedance at the injector face plate is infinitely high.
- 4) The mean flow in baffle compartments is neglected.

The impedance at the baffle edge is defined as

$$Z_c = \frac{S_c p'}{u'} \quad (\text{A17})$$

where S_c denotes the cross-sectional area of the combustion chamber. Substituting Eqs. (14–16) into Eq. (A17) and manipulating the result yields

$$Z_c = i \frac{S_c \bar{\rho}_c \bar{a}_c \Omega}{\sqrt{k_{mn}^2 \bar{a}_c^2 - \Omega^2}} = i \frac{S_c \bar{\rho}_c \bar{a}_c \bar{\Omega}_{mn}}{\sqrt{1 - \bar{\Omega}_{mn}^2}} \quad (\text{A18})$$

where $\bar{\Omega}_{mn} = \Omega/(k_{mn} \bar{a}_c)$ is the normalized frequency of the (m, n) th mode.

Because pure longitudinal oscillations are assumed in baffle compartments, the acoustic impedance at the baffle exit can be determined from Eq. (A8),

$$Z_b = S_b \bar{\rho}_b \bar{a}_b \frac{\bar{Z}_0 + i \tan(kL_b)}{i\bar{Z}_0 \tan(kL_b) + 1} \quad (\text{A19})$$

where S_b denotes the cross-sectional area of the baffle compartments and $k = \Omega/\bar{a}_b$. Application of the condition $\bar{Z}_0 \rightarrow \infty$ to Eq. (A19) results in

$$Z_b = -i S_b \bar{\rho}_b \bar{a}_b / \tan(kL_b) \quad (\text{A20})$$

Defining the normalized baffle length $\bar{L}_b = L_b/R_c$ and the ratio of sound velocities in the compartments to that in the main chamber $\alpha_b = \bar{a}_b/\bar{a}_c$, the following is obtained:

$$kL_b = R_c k_{mn} \bar{L}_b \bar{\Omega}_{mn} / \alpha_b \quad (\text{A21})$$

Equation (A21) is substituted into Eq. (A20) to acquire

$$Z_b = \frac{-i S_b \bar{\rho}_b \bar{a}_b}{\tan(R_c k_{mn} \bar{L}_b \bar{\Omega}_{mn} / \alpha_b)} \quad (\text{A22})$$

The imaginary part of the impedance taken from the chamber inlet in the positive x direction is equal to that taken from the chamber exit in the negative x direction. This condition can be written as

$$iY(x) = iY(L - x) \quad (\text{A23})$$

where $Y(x)$ is the imaginary part of the transposed impedance as a function of the axial coordinate x . Applying this condition to Eqs. (A18) and (A22), the frequency of acoustic waves in baffled combustion chambers is obtained.

$$\tan\left(\frac{R_c k_{mn} \bar{L}_b \bar{\Omega}_{mn}}{\alpha_b}\right) = \frac{S_c \bar{\rho}_c \bar{a}_c \bar{\Omega}_{mn}}{S_b \bar{\rho}_b \bar{a}_b \sqrt{1 - \bar{\Omega}_{mn}^2}} \quad (\text{A24})$$

References

- [1] Harrje, D. T., and Reardon, F. H., "Liquid Propellant Rocket Combustion Instability," NASA SP-194, 1972.
- [2] Yang, V., and Anderson, W., *Liquid Rocket Engine Combustion Instability*, Vol. 169, Progress in Astronautics and Aeronautics, AIAA, Washington, D.C., 1995.
- [3] Dranovsky, M., Yang, V., Culick, F. E. C., and Talley, D. G., *Combustion Instabilities in Liquid Rocket Engines: Testing and Development Practices in Russia*, Vol. 221, Progress in Astronautics and Aeronautics, AIAA, Reston, VA, 2007.
- [4] Lieuwen, T. C., and Yang, V., *Combustion Instabilities in Gas Turbine Engines: Operational Experience, Fundamental Mechanisms and Modeling*, Vol. 210, Progress in Astronautics and Aeronautics, AIAA, Reston, VA, 2005.
- [5] Culick, F. E. C., and Yang, V., "Prediction of the Stability of Unsteady Motions in Solid Propellant Rocket Motors," *Nonsteady Burning and Combustion Stability of Solid Propellants*, edited by DeLuca, L., and Summerfield, M., Vol. 143, Progress in Astronautics and Aeronautics, AIAA, Washington, D.C., 1992, pp. 719–779, Chap. 18.
- [6] *Solid-Propellant Chemistry, Combustion, and Motor Interior Ballistics*, edited by Yang, V., Brill, T., and Ren, W. Z., Vol. 185, Progress in Astronautics and Aeronautics, AIAA, Reston, VA, 2000.
- [7] Male, T., and Kerslake, W. R., "A Method of Prevention of Screaming in Rocket Engines," NASA RM-E54F28A, 1954.
- [8] Wieber, P. R., "Acoustic Decay Coefficients of Simulated Rocket Chambers," NASA TN-D-3425, 1966.
- [9] Torda, T. P., and Patel, B. R., "Analytical and Experimental Investigation of Oscillations in Rocket Motor Baffle Cavities," Air Force Office of Scientific Research Report 68-1369, Arlington, VA, 1968.
- [10] Hannum, N. P., Bloomer, H. E., and Goelz, R. R., "Stability Effects of Several Injector Face Baffle Configurations on Screech in Hydrogen-Oxygen Rocket," NASA TN-D-4515, 1968.
- [11] Laudien, E., Pongratz, R., Pierro, R., and Preklik, D., "Experimental Procedures Aiding the Design of Acoustic Cavities," *Liquid Rocket Engine Combustion Instability*, edited by Yang, V., and Anderson, W. E., Vol. 169, Progress in Astronautics and Aeronautics, AIAA, Washington, D.C., 1995, pp. 377–399.
- [12] Fung, Y. T., Yang, V., and Sinha, A., "Active Control of Combustion Instabilities with Distributed Actuators," *Combustion Science and Technology*, Vol. 78, Nos. 4–6, 1991, pp. 217–245. doi:10.1080/00102209108951750
- [13] Fung, Y. T., and Yang, V., "Active Control of Nonlinear Pressure Oscillations in Combustion Chambers," *Journal of Propulsion and Power*, Vol. 8, No. 6, 1992, pp. 1282–1289.
- [14] Oefelein, J. C., and Yang, V., "A Comprehensive Review of Liquid-Propellant Combustion Instabilities in F-1 Engines," *Journal of Propulsion and Power*, Vol. 9, No. 5, 1993, pp. 657–677. doi:10.2514/3.23674
- [15] Lee, K. J., Kim, H. J., Seo, S., and Choi, H. S., "Experimental Verification for Acoustic Damping Enhancement by Gaps in Injector-Formed Baffles," *Journal of Propulsion and Power*, Vol. 25, No. 2, 2009, pp. 435–442. doi:10.2514/1.40589
- [16] Lubarsky, E., Hadjipanayis, M., Shcherbik, D., Bibik, O., and Zinn, B. T., "Control of Tangential Instability by Asymmetric Baffle," AIAA Paper 2008-955, 2008.
- [17] Sirignano, W. A., "Design Factors Affecting Damping," *Liquid Propellant Rocket Engines*, edited by Harrje, D. T., and Reardon, F. H., NASA SP-194, 1972, pp. 385–399.
- [18] Combs, L. P., Oberg, C. L., Coultas, T. A., and Evers, W. H., "Liquid Rocket Engine Combustion Stabilization Devices," NASA SP-8113, 1974.
- [19] Wicker, J. M., Yoon, M. W., and Yang, V., "Linear and Non-Linear Pressure Oscillations in Baffled Combustion Chambers," *Journal of Sound and Vibration*, Vol. 184, No. 1, 1995, pp. 141–171. doi:10.1006/jsvi.1995.0309
- [20] Acker, T. L., Cody, J. D., and Mitchell, C. E., "Acoustic Oscillations in a Cylindrical Chamber with a Hub Baffle," AIAA Paper 99-1977, 1999.
- [21] Natanzon, M. S., *Combustion Instability*, edited by Culick, F. E. C., Vol. 222, Progress in Astronautics and Aeronautics, AIAA, Reston, VA, 2008.
- [22] Quinlan, J. M., Kirkpatrick, A. T., Milano, D., Mitchell, C. E., and Hinerman, T. D., "Analytical and Numerical Development of a Baffled Liquid Rocket Combustion Stability Code," *Journal of Propulsion and Power*, Vol. 28, No. 1, 2012, pp. 122–131. doi:10.2514/1.B34276
- [23] Feng, S., Nie, W., He, B., and Zhuang, F., "Control Effects of Baffle on Combustion Instability in a LOX/GH2 Rocket Engine," *Journal of Spacecraft and Rockets*, Vol. 47, No. 3, 2010, pp. 419–426. doi:10.2514/1.46240
- [24] Quinlan, J. M., Bibik, O., and Zinn, B. T., "Experimental and Numerical Combustion Instability Modes in Asymmetric Baffled Chambers," AIAA Paper 2010-6802, 2010.
- [25] Culick, F. E. C., and Yang, V., "Overview of Combustion Instabilities in Liquid-Propellant Rocket Engines," *Liquid Rocket Engine Combustion Instability*, edited by Yang, V., and Anderson, W. E., Vol. 169, Progress in Astronautics and Aeronautics, AIAA, Washington, D.C., 1995, pp. 3–37, Chap. 1.
- [26] You, D., and Yang, V., "Three-Dimensional Linear Stability Analysis of Gas Turbine Combustors," *Combustion Instabilities in Gas Turbine Engines*, edited by Lieuwen, T., and Yang, V., Vol. 210, Progress in Astronautics and Aeronautics, AIAA, Reston, VA, 2005, pp. 415–443, Chap. 14.
- [27] Yang, V., Kim, S. I., and Culick, F. E. C., "Triggering of Longitudinal Pressure Oscillations in Combustion Chambers I: Nonlinear Gasdynamics," *Combustion Science and Technology*, Vol. 72, Nos. 4–6, 1990, pp. 183–214. doi:10.1080/00102209008951647
- [28] Yang, V., and Culick, F. E. C., "On the Existence and Stability of Limit Cycles for Transverse Acoustic Modes in a Cylindrical Combustion Chamber I: Standing Modes," *Combustion Science and Technology*, Vol. 72, Nos. 1–3, 1990, pp. 37–65. doi:10.1080/00102209008951639
- [29] Wicker, J. M., Greene, W. D., Seung, K., III, and Yang, V., "Triggering of Longitudinal Combustion Instabilities in Rocket Motors: Nonlinear Combustion Response," *Journal of Propulsion and Power*, Vol. 12, No. 6, 1996, pp. 1148–1158. doi:10.2514/3.24155
- [30] Crocco, L., and Cheng, S. I., "Theory of Combustion Instability in Liquid Propellant Rocket Motors," *AGARD Monograph No. 8*, Butterworths Scientific Publ., London, 1956.
- [31] You, D., Huang, Y., and Yang, V., "A Generalized Model of Acoustic Response of Turbulent Premixed Flame and Its Application to Gas-Turbine Combustion Instability Analysis," *Combustion Science and Technology*, Vol. 177, Nos. 5–6, 2005, pp. 1109–1150. doi:10.1080/00102200590927012

E. Kim
Associate Editor